Journal of Hydrology 602 (2021) 126797

Contents lists available at ScienceDirect

Journal of Hydrology

journal homepage: www.elsevier.com/locate/jhydrol

A two-layer numerical model of soil moisture dynamics: Model development

Junhao He [a,*], Mohamed M. Hantush [b], Latif Kalin [c], Mehdi Rezaeianzadeh [d], Sabahattin Isik [e]

[a] School of Forestry and Wildlife Sciences, 602 Duncan Drive, Auburn, AL 36849, USA
[b] U.S. EPA the Center for Environmental Solutions and Emergency Response, 26 West Martin Luther King Dr., Cincinnati, OH 45268, USA
[c] School of Forestry and Wildlife Sciences, 602 Duncan Drive, Auburn, AL 36849, USA
[d] Lynker Technologies, LLC, Boulder, CO 80301, USA
[e] School of Forestry and Wildlife Sciences, 602 Duncan Drive, Auburn, AL 36849, USA

ARTICLE INFO

This manuscript was handled by Corrado Corradini, Editor-in-Chief, with the assistance of Wei Hu, Associate Editor

Keywords:
Richards equation
Model
Soil moisture
Root zone
Vadose soil
Evapotranspiration

ABSTRACT

Simulating water moisture flow in variably saturated soils with a relatively shallow water table is challenging due to the high nonlinear behavior of Richards' equation (RE). A two-layer approximation of RE was derived in this paper, which describes vertically-averaged soil moisture content and flow dynamics in the root zone and the unsaturated soil below. To this end, the partial differential equation (PDE) describing RE was converted into two-coupled ordinary differential equations (ODEs) describing dynamic vertically-averaged soil moisture variations in the two soil zones subject to a deep or shallow water table in addition to variable soil moisture flux and pressure conditions at the surface. The coupled ODEs were solved numerically using the iterative Huen's method for a variety of flux and pressure-controlled top and bottom boundary conditions (BCs). The numerical model was evaluated for three typical soil textures with free-drainage and mixed flux-pressure head at the bottom boundary under various atmospheric conditions. The results of soil water contents and fluxes were validated using HYDRUS-1D as a benchmark. Simulated values showed that the new model is numerically stable and generally accurate in simulating vertically-averaged soil moisture in the two layers under various flux and prescribed pressure BCs. A hypothetical simulation scenario involving desaturation of initially saturated soil profile caused by exponentially declining water table demonstrated the robustness of the numerical model in tracking vertically-averaged moisture contents in the roots layer and the lower vadose soil as the water table continued to fall. The two-layer model can be used by researchers to simulate variably saturated soils in wetlands and by water resources planners for efficient coupling of land-surface systems to groundwater and management of conjunctive use of surface and groundwater.

1. Introduction

Soil moisture distribution and fluxes are fundamental components in the hydrological cycle. They connect surface water and groundwater and function as a source for evaporation demand, including plant transpiration (Maxwell and Condon, 2016). Besides, soil moisture is also known to control terrestrial biogeochemical processes by regulating the soil microbial respiration (Orchard and Cook, 1983; Liu et al., 2009). Soil moisture and fluxes should be well represented by hydrological and biogeochemical models as they play important roles for water resources planning and management and tracking water and solute mass budgets of a watershed.

One of the fundamental and well-known equations to describe unsaturated flow in porous media is Richard's Equation (hereafter RE) (Richards, 1931). It is often used to represent the physics of water distribution and flow in soils (root and vadose zones) by the forces of capillarity and gravity at the local-field and watershed scales. The RE is obtained by substituting Darcy's equation into the continuity equation and considering applicable sink/source terms. The one-dimensional form of RE can be written as

$$\frac{\partial \theta}{\partial t} = -\frac{\partial}{\partial z}\left[K(\theta)\left(\frac{\partial \psi}{\partial z}+1\right)\right] - S(z) \quad (1)$$

where θ is the volumetric water content [L^3L^{-3}]; K is unsaturated hydraulic conductivity [LT^{-1}]; ψ is capillary pressure head (negative of soil

* Corresponding author.
E-mail addresses: jzh0126@auburn.edu (J. He), hantush.mohamed@epa.gov (M.M. Hantush), kalinla@auburn.edu (L. Kalin), szi0003@auburn.edu (S. Isik).

https://doi.org/10.1016/j.jhydrol.2021.126797
Received 22 November 2020; Received in revised form 2 August 2021; Accepted 5 August 2021
Available online 13 August 2021

water pressure head) [L]; t is time [T]; S is a sink term for plant roots' uptake [T^{-1}]; and z is the vertical coordinate [L] (positively oriented downward).

RE is known as a highly nonlinear, elliptic–parabolic partial differential equation (PDE). Although numerous studies have been done to address the non-linearity of RE, obtaining an accurate and efficient numerical solution of RE has remained challenging (Farthing and Ogden, 2017). Besides, RE is coupled with two empirical, highly nonlinear soil hydraulic functions: unsaturated hydraulic conductivity function $K(\theta)$ and soil–water characteristic curve $\psi(\theta)$. A condition known as degeneration can be introduced to the solution of RE when either or both of the values of unsaturated hydraulic conductivity and capillary-pressure head are close to zero (List and Radu, 2016). Algorithms have been developed for solving RE numerically in saturated and unsaturated flow problems. Various numerical solutions of RE have been proposed using spatial and temporal discretization schemes in methods of finite differences (Celia et al., 1990; Ross, 1990; Rathfelder and Abriola, 1994; Herrada et al., 2014), finite volume (Kumar et al., 2009; Caviedes-Voullième et al., 2013; Lai and Ogden, 2015; and Svyatskiy and Lipnikov, 2017), and finite element (Forsyth et al., 1995; Lee and Abriola, 1999; Šimůnek et al., 2005). Ross (1990) presented an efficient finite difference scheme for solving RE using hyperbolic Sine transformation of matric potential considering soil infiltration. Caviedes-Voullième et al. (2013) applied an implicit finite volume scheme based on the mixed form of RE and implemented Celia et al. (1990) method to infiltration and column drainage flow scenarios. They concluded that this scheme is mass conservative and can solve the equation under saturated conditions and when soil transitions from unsaturated to saturated conditions. Further, for numerical stability and efficiency, it is better to use relatively large time steps with coarse meshes. Varado et al. (2006) expressed flux in terms of matrix (Kirchoff) potential and presented and validated a finite difference scheme expressed in terms of soil saturation. Besides demonstrating efficiency of the numerical solution, they concluded that it is necessary to use finer spatial discretization near the soil surface for accurately modeling the cumulative infiltration in fine-textured soils. Despite these efforts and many others, the spatial and temporal discretization of RE continue to pose a challenge, especially for soils with initially low moisture contents and high heterogeneity due to mass balance errors and numerical oscillation and dispersion (e.g., Belfort et al., 2013; and Caviedes-Voullième et al., 2013).

Although application of RE at the laboratory and field scales has been relatively successful (Lai and Ogden, 2015; Liu et al., 2018; Zha et al., 2013), application of RE to larger scale systems such as wetlands and watersheds can be even more challenging. Using the numerical scheme proposed by van Dam and Feddes (2000), Sharifi et al. (2017) reported the frequent crashing of the RE solver, especially when soil is near saturation. In that study, high resolution of soil moisture values with depth was irrelevant and only layer-average values were important in simulating nitrogen and carbon cycling. Contemporary medium or large-scale soil moisture models often consider simplified representation of RE for moisture dynamics to decrease the computational burden. Some examples to this include RE coupled mass conservation equation (Zhu et al., 2016), analytical solution of RE (Huang and Wu, 2012; Su et al., 2018), coarse finite difference resolution (Downer and Ogden, 2004a; Downer and Ogden, 2004b), and simpler functions for water retention parameters (Hayek, 2016).

Watershed and land surface models often rely on average soil moisture content than point values to simulate energy balance and biochemical processes such as CLM (Oleson et al., 2010), GSSHA (Downer and Ogden, 2004a; Downer and Ogden, 2004b) and SVAT (Sellers et al., 1986). In these approaches, average moisture content for each soil layer is calculated either by integrating computed soil moisture over the layer or by selecting a nodal value to represent the average soil moisture content. Although RE estimates soil moisture from a physical perspective, the numerical schemes can be unstable and computational cost can increase exponentially at such scales. This is especially true when a solution is required over large areas and repetitive model simulations are needed to quantify model predictive uncertainty using, e.g., Monte Carlo simulations. Moreover, estimation of soil moisture values at high vertical resolution might be redundant and unnecessary (Cao and Yue, 2014) and can be unreliable in some applications (Farthing et al., 2003). Although several simplified approaches have been proposed to calculate moisture content for certain depth of soil in watershed scale applications, such as the soil water balance bucket model (Sanchez-Mejia and Papuga, 2017), these approaches cannot account for the complexities of soil water movement as RE does. Therefore, a stable and efficient numerical solution of RE is needed for large-scale soil moisture estimations and when modeling the coupling land surface and surface water to groundwater. The solution should be able to deal with the interactions between unsaturated soil and fluctuating groundwater levels by the actions of recharge, accretion or evaporative losses. Furthermore, a numerical scheme should be designed to approximate vertically-averaged volumetric soil moisture content with some mathematical rigor, with quantifiable errors to eliminate the need for high-resolution details and thus reduce computational resource usage in terms of computation time and memory storage.

Despite presenting integrated form of Eq. (1) (e.g., Lee and Abriola, 1999; Herrada et al., 2014; and Lai and Ogden, 2015), analyses often proceeded with essentially finite-differences approximation of point values. All these schemes were proposed to obtain solutions at high vertical resolution, by discretizing the flow domain into multiple numerical cells. They are not designed to obtain moisture content averaged over vertically delineated soil layers (e.g., root zone and intermediate vadose zone), unless solutions are further processed. Worth noting is the work by Kumar (2004) where RE was averaged over a sloping soil to describe depth-averaged mean moisture content considering the effect of soil heterogeneity. The analysis emphasized relative contributions of various components of the lateral flow, but a solution was not presented and verified. While much of the literature has focused on numerical algorithms for solving RE at the point scale, much less effort has been devoted to the solution of layer-averaged forms with emphases on numerical efficiency and presence of water table at relatively shallow depth.

The interaction between saturated and unsaturated zone plays a critical role in the hydrological cycle (Zeng and Decker, 2009; Bizhanimanzar et al., 2019; Dai et al., 2019). Water table fluctuations can affect soil moisture in the root zone and regulate soil evaporation and plant water uptake (Sulis et al., 2011). During dry periods, soil profile can receive upward water flux from the water table, which could potentially be a crucial source of water to plants. The interactions between unsaturated (typically root zone) and saturated zone can be one-directional when water table is relatively deep (e.g., Celia et al., 1990; Varado et al., 2006; Herrada et al., 2014; Lai and Ogden, 2015; Hayek, 2016; Zhang et al., 2016; Rahman et al., 2019), and two-directional when the water table is relatively shallow and has significant effects on the water storage in the vadose soil. The numerical solution of RE becomes degenerate when the water table is within the root zone and close to the surface (Ogden et al., 2017). This further underscores the need for a stable, efficient and operational numerical model that can couple soil surface to groundwater and simulate saturation and desaturation close to the surface under highly variable climate conditions and fluctuating water table.

This paper presents a new numerical model for two-layer vertically-averaged RE describing one-dimensional vertical water movement in the root zone and the vadose layer below. The solution is derived from first-order approximation (truncated error of order $(\Delta z)^2$) of vertically-averaged soil moisture content and the mixed form of RE. It converts the PDE to two-coupled ODEs describing vertically-averaged moisture content and flow in two layers. The numerical model considers various atmospheric conditions along with plant water uptake and water movement between soil and fluctuating water table. The objectives of

this paper are to: 1) derive a vertically-averaged and mass-conservative approximation of RE; 2) verify the model performance by comparison with the reference model HYDRUS considering various types of BCs; and 3) demonstrate the capability of the model in simulating the presence of a dynamic water table. The overarching goal is to develop a numerically stable and efficient module for field and watershed-scale soil moisture and flux simulations.

2. Methodology

2.1. Water table below the root zone layer (two-layer model)

The equation governing one-dimensional vertical water movement in soils is the flow continuity equation:

$$\frac{\partial \theta}{\partial t} = -\frac{\partial q}{\partial z} - S \tag{2}$$

where, θ is volumetric water content [L^3L^{-3}]; t is time [T]; z is soil depth below the surface [L], positive downward; S is a soil moisture sink term (e.g. plant transpiration) [$L^3L^{-3}T^{-1}$]; and q is flux per unit area [$L^3T^{-1}L^{-2}$], given by Darcy's law:

$$q = K\frac{\partial \psi}{\partial z} + K \tag{3}$$

where, K is unsaturated hydraulic conductivity [LT^{-1}]; and ψ is negative of soil pressure head (capillary pressure head or matric potential) [L].

Fig. 1 is a schematic illustration of a soil profile with a root zone of thickness h and water table at depth $H(t)$ and time t. Two layers are delineated; the first layer with thickness h denotes the root zone. The second layer with thickness (H-h) corresponds to vadose soil extending from the bottom of the first layer to the water table. We derive coupled ODEs of average moisture contents $\bar{\theta}_1$ and $\bar{\theta}_2$ for the root zone layer and the second layer, respectively. First, let us assume groundwater level is initially below the first layer ($H(t) > h$), $\bar{\theta}_1$ and $\bar{\theta}_2$ are defined as

$$\bar{\theta}_1(t) = \frac{1}{h}\int_0^h \theta(z,t)dz \tag{4}$$

$$\bar{\theta}_2(t) = \frac{1}{H(t)-h}\int_h^{H(t)} \theta(z,t)dz \tag{5}$$

We start by integrating Eq. (2) from z = 0 to z = h:

$$\int_0^h \frac{\partial \theta}{\partial t}dz = -\int_0^h \frac{\partial q}{\partial z}dz - \int_0^h Sdz \tag{6}$$

which yields

$$h\frac{d\bar{\theta}_1}{dt} = q|_{z=0} - q\,\big|_{z=h} - h\bar{S} \tag{7}$$

where, $q|_{z=0}$ is flux at soil surface [LT^{-1}]; $q|_{z=h}$ is interface flux between the first layer and the second layer [LT^{-1}]; and $\bar{S}$ is average transpiration rate over the root zone [$L^3L^{-3}T^{-1}$]: $\bar{S} = \int_0^h Sdz/h$. Integrating (2) over the second layer, from $z = h$ to $z = H(t)$, and taking out the S term

$$\int_h^{H(t)} \frac{\partial \theta}{\partial t}dz = -\int_h^{H(t)} \frac{\partial q}{\partial z}dz \tag{8}$$

and applying the Leibnitz rule yields

$$(H-h)\frac{d\bar{\theta}_2}{dt} - \theta_{2s}\frac{dH}{dt} = q|_{z=h} - q|_{z=H} \tag{9}$$

where, θ_{2s} is the saturated moisture content of the second layer [L^3L^{-3}];

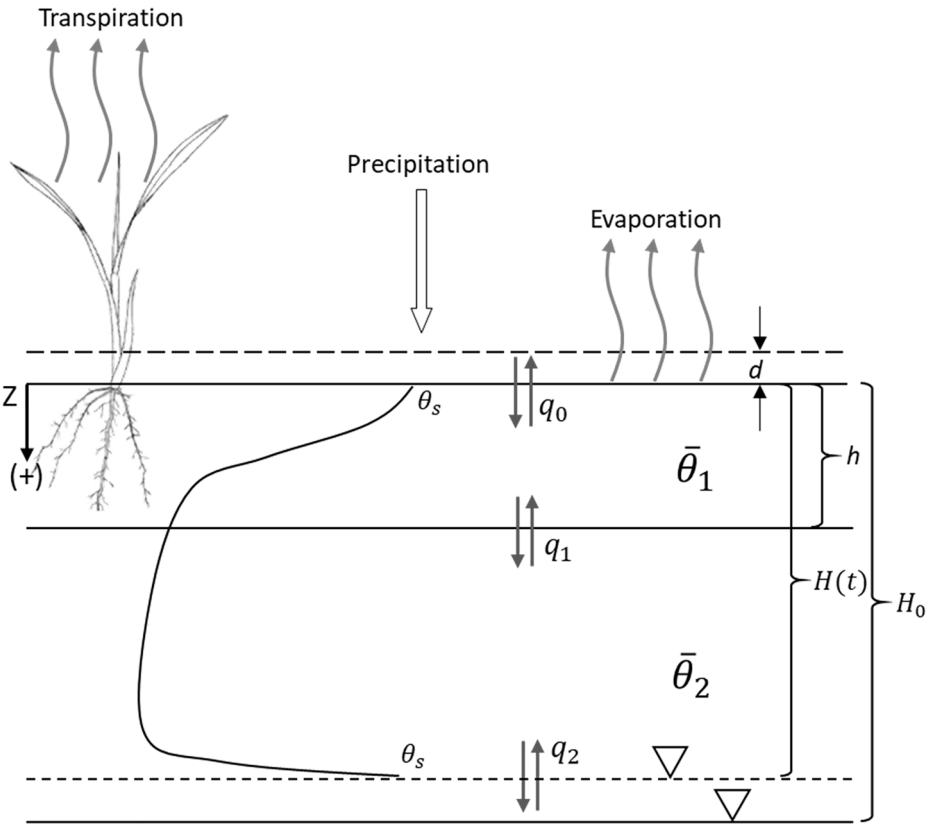

Fig. 1. Schematic illustration of soil profile and the two-layer model depicting the root zone and vadose soil below. d is the ponding depth; h is the first layer (zoot zone) depth; $H(t)$ is depth of WT at time t; and H_0 is initial depth; q_0, q_1 and q_2 are the top, middle and bottom flux (positive downward), respectively.

$q|_{z=H}$ is the flux at bottom of the second layer [LT^{-1}].

At the interface of two layers ($z = h$), $q|_{z=h}$ is given by:

$$q|_{z=h} = K|_{z=h}\left.\frac{\partial\psi}{\partial z}\right|_{z=h} + K|_{z=h} \tag{10}$$

Taylor series expansion of ψ around $z = h$ is

$$\psi(z,t) = \psi(h,t) + \left.\frac{\partial\psi}{\partial z}\right|_{z=h}(z-h) + \frac{1}{2}\left.\frac{\partial^2\psi}{\partial z^2}\right|_{z=h}(z-h)^2 + \cdots \tag{11}$$

Integrating (11) from $z = 0$ to $z = h$ and retaining zero and first-order terms yield

$$\overline{\psi}_1 \cong \psi(h,t) - \frac{1}{2}\left.\frac{\partial\psi}{\partial z}\right|_{z=h} h \tag{12}$$

thus,

$$\left.\frac{\partial\psi}{\partial z}\right|_{z=h} \cong 2\frac{\psi(h,t) - \overline{\psi}_1}{h} \tag{13}$$

where, $\overline{\psi}_1$ is the average of $\psi_1$in the first layer [L], $\overline{\psi}_1 = \int_0^h \psi(z,t)dz/h$.

Integrating (11) from $z = h$ to $z = H$ and dropping higher-order terms yields

$$\overline{\psi}_2 \cong \psi(h,t) + \frac{1}{2}\left.\frac{\partial\psi}{\partial z}\right|_{z=h}(H-h) \tag{14}$$

Hence,

$$\left.\frac{\partial\psi}{\partial z}\right|_{z=h} \cong 2\frac{\overline{\psi}_2 - \psi(h,t)}{H-h} \tag{15}$$

where, $\overline{\psi}_2 = \int_h^H \psi(z,t)dz/(H-h)$. Eqs. (13) and (15) lead to this approximation:

$$2\frac{\psi(h,t) - \overline{\psi}_1}{h} = 2\frac{\overline{\psi}_2 - \psi(h,t)}{H-h} \tag{16}$$

which can be solved for $\psi(h,t)$,

$$\psi(h,t) = \beta\overline{\psi}_1 + (1-\beta)\overline{\psi}_2 \tag{17}$$

where, $\beta = \frac{H-h}{H}$, $1-\beta = \frac{h}{H}$.

Substituting (17) into either (12) or (14) yields

$$\left.\frac{\partial\psi}{\partial z}\right|_{z=h} = \frac{2}{H}\left(\overline{\psi}_2 - \overline{\psi}_1\right) \tag{18}$$

Using the Taylor-series expansion of K around $z = h$:

$$K(z,t) = K(h,t) + \left.\frac{\partial K}{\partial z}\right|_{z=h}(z-h) + \frac{1}{2}\left.\frac{\partial^2 K}{\partial z^2}\right|_{z=h}(z-h)^2 + \cdots \tag{19}$$

Similarly, by integrating (19) from $z = 0$ to $z = h$ and dropping higher-order terms, one can show

$$\left.\frac{\partial K}{\partial z}\right|_{z=h} = 2\frac{K(h,t) - \overline{K}_1}{h} \tag{20}$$

where, $\overline{K}_1 = \int_0^h K(z,t)dz/h$. Hereafter, we make the approximation $\overline{K}_1 \cong K_1(\overline{\theta}_1)$.

Integrating (19) from $z = h$ to $z = H$ and dividing by $(H-h)$ yields

$$\left.\frac{\partial K}{\partial z}\right|_{z=h} = 2\frac{\overline{K}_2 - K(h,t)}{H-h} \tag{21}$$

where, $\overline{K}_2 = \int_h^H K(z,t)dz/(H-h) \cong K_2\left(\overline{\theta}_2\right)$.

Comparison of (20) with (21) leads to

$$2\frac{K(h,t) - \overline{K}_1}{h} = 2\frac{\overline{K}_2 - K(h,t)}{H-h} \tag{22}$$

Hence,

$$K(h,t) = \beta\overline{K}_1 + (1-\beta)\overline{K}_2 \tag{23}$$

Underlying Eq. (23) is the assumption that $K(z,t)$ is a continuous function and differentiable with respect to z.

Substituting (18) and (23) into (10) yields this expression for $q|_{z=h}$:

$$q|_{z=h} = \frac{2}{H}\left(\beta\overline{K}_1 + (1-\beta)\overline{K}_2\right)\left(\overline{\psi}_2 - \overline{\psi}_1\right) + \beta\overline{K}_1 + (1-\beta)\overline{K}_2 \tag{24}$$

The top flux $q|_{z=0}$ is controlled by precipitation and evaporation,

a) If $i > 0$ and $i < K_{s1}$,

$$q|_{z=0} = i \tag{25}$$

where, K_{s1} is saturation conductivity of the first layer [LT^{-1}]; and i is precipitation rate [LT^{-1}].

b) If $i > 0$ and $i > K_{s1}$, Eq. (25) holds until the first layer is saturated. Ponding occurs immediately after the first layer is saturated. If the ponding depth is d [L], we have

$$q|_{z=0} = 2K_{s1}\frac{\overline{\psi}_1 + d}{h} + K_{s1} \tag{26}$$

c) If $i = 0$,

$$q|_{z=0} = -ev_a \tag{27}$$

where, ev_a is soil actual evaporation rate [LT^{-1}].

At $z = H$, flux to the water table is

$$q|_{z=H} = K|_{z=H}\left.\frac{\partial\psi}{\partial z}\right|_{z=H} + K|_{z=H} \tag{28}$$

and

$$K|_{z=H} = K_{s2} \tag{29}$$

Once again, we expand ψ around $z = H$ and integrate from z = h to z = H to obtain

$$\left.\frac{\partial\psi}{\partial z}\right|_{z=H} = 2\frac{\psi(H,t) - \overline{\psi}_2}{H-h} \tag{30}$$

Let $\psi(H,t) = \psi_b$, where ψ_b is the critical bubbling suction (i.e., negative of air-entry capillary pressure) of the soil. Thus,

$$q|_{z=H} = 2K_{s2}\frac{\psi_b - \overline{\psi}_2}{H-h} + K_{s2} \tag{31}$$

If water table drops deep below H, free drainage condition holds at the bottom and $\left.\frac{\partial\psi}{\partial z}\right|_{z=H} = 0$. It can be shown using Taylor-series expansion of K around $z = H$ and noting that $\left.\frac{\partial K}{\partial z}\right|_{z=H} = 0$ for free drainage BC, that to the first-order, flux $q|_{z=H}$ becomes

$$q|_{z=H} = \overline{K}_2 \cong K_2\left(\overline{\theta}_2\right) \tag{32}$$

Eqs. (7) and (9) with flux expressions (24–27) and (31), and interface expressions (17) and (23) collectively form two-coupled ordinary differential equations describing the dynamics of average volumetric water content in the root zone and the lower vadose soil bounded by the water table at the bottom. Hereafter, we refer to Eqs. (7) and (9) with (24) and (31) as the two-layer model.

2.2. Water table within the first layer (one-layer model)

Here, we address the case where groundwater level is within the root zone (first soil layer), $0 < H \leq h$. The average water content in the root zone is calculated by a weighted average of moisture content in both the saturated and unsaturated parts:

$$\overline{\theta}_1(t) = \frac{H\overline{\theta}_{1u}(t) + (h-H)\theta_{1s}(t)}{h} \tag{33}$$

where, $\overline{\theta}_{1u}$ is moisture content of unsaturated part of the first layer [L^3L^{-3}], θ_{1s} is saturation water content of the first layer [L^3L^{-3}].

$\overline{\theta}_{1u}(t)$ is defined as

$$\overline{\theta}_{1u}(t) = \frac{1}{H(t)}\int_0^{H(t)} \theta(z,t)dz \tag{34}$$

Following similar steps, Integration of Eq. (2) from z = 0 to z = $H(t)$ yields

$$H\frac{d\overline{\theta}_{1u}}{dt} - \theta_{1s}\frac{dH}{dt} = q|_{z=0} - q\,|_{z=H} - H\overline{S}_u \tag{35}$$

where, $q|_{z=H}$ is flux at the water table [LT^{-1}]; and $\overline{S}_u = \int_0^H Sdz/H$.

Similar to (31), $q|_{z=H}$ to the first-order is given by

$$q|_{z=H} = 2K_{s1}\frac{\psi_b - \overline{\psi}_{1u}}{H} + K_{s1} \tag{36}$$

where, $\overline{\psi}_{1u}$ is capillary pressure head of the unsaturated part of the first layer [L].

The time-dependent H and dH/dt terms account for the expansion and contraction of the layers over which $\overline{\theta}_1$ and $\overline{\theta}_2$ are computed. In this scenario, the two layers are virtual and not physical; they cease to exist when the water table rises to the surface and the entire soil profile is saturated. The first layer evolves from zero thickness to $H(t)$ until the water table drops to the level lower than the root zone, where thickness becomes constant at h. The second layer then start evolving from zero thickness and expands to $H(t)$-h as the water table continues to fall.

2.3. Unsaturated soil hydraulic properties

The two-layer model uses the Van Genuchten (1980) model for the soil hydraulic characteristic relationships ψ and K:

$$K(S_e) = \begin{cases} K_s S_e^{\lambda}\left[1 - \left(1 - S_e^{\frac{1}{m}}\right)^m\right]^2 & \psi < 0 \\ K_s & \psi \geq 0 \end{cases} \tag{37}$$

$$\psi(S_e) = \frac{1}{\alpha}\left(S_e^{-\frac{1}{m}} - 1\right)^{1-m} \tag{38}$$

$$S_e = \frac{\theta - \theta_r}{\theta_s - \theta_r} \tag{39}$$

$$m = 1 - \frac{1}{n} \tag{40}$$

where, θ_r and θ_s are residual and saturated water content, respectively [L^3L^{-3}], K_s is saturated hydraulic conductivity [LT^{-1}], S_e is effective saturation rate [–], n is an empirical shape-defining parameter [–], λ is the pore size distribution index [–] and α is a fitting parameter [L^{-1}].

2.4. Transpiration estimation

The sink term S, which is defined as the volume of water removed from a unit volume of soil per unit time due to plant water uptake, is calculated using the water stress function proposed by Feddes (1982),

$$S(\psi) = \gamma(\psi)S_p \tag{41}$$

where, $\gamma(\psi)$ is soil water stress response function of the soil matric potential ($0 \leq \gamma \leq 1$) and S_p is potential plant transpiration rate [T^{-1}]. The plant water uptake is calculated by a water stress response function as shown in Fig. 2. When soil is approaching saturation with matric potential higher than ψ_1 or losing water to the point matric potential is below ψ_4, plant water uptake ceases ($\gamma = 0$). Water uptake is equal to the potential rate when soil matric potential is between certain predefined capillary pressure heads (ψ_2 and ψ_3). As for matric potential between ψ_1 and ψ_2 (or ψ_3 and ψ_4), water uptake is calculated as linearly increasing (or decreasing) with ψ.

2.5. Evaporation estimation

Evaporation is calculated from potential evaporation for water content of the first layer greater than wilting point using the relationship,

$$ev_a = ev_p\left(\frac{\overline{\theta}_1 - \theta_{wp}}{\theta_{fc} - \theta_{wp}}\right)^p \tag{42}$$

where, ev_p is potential evaporation rate [LT^{-1}], θ_{wp} is moisture content at wilting point (−1500 kPa) [L^3L^{-3}], θ_{fc} is volumetric water content at field capacity (−33 kPa) [L^3L^{-3}] and p is an exponent coefficient [–]. The value of p was set to 1. Potential transpiration rate (S_p) and potential evaporation rate (ev_p) can be calculated by partitioning of potential evapotranspiration calculated either by process-based or empirical equations, such as Penman-Monteith method (Allen et al., 2005), Hargreaves equation (Jensen et al., 1997) and Priestley-Taylor equation (Priestley and Taylor, 1972).

2.6. Numerical scheme

The governing Eqs. (7) and (9) with (24) and (31) for the two-layer model are solved explicitly by using the predictor–corrector algorithm Heun's method (Chapra and Canale, 2015). First, the fluxes q_n (q_0 refers to the top flux $q|_{z=0}$, q_1 refers to the interface flux of two layers $q|_{z=h}$ and q_2 refers to bottom flux $q|_{z=H}$) at the boundaries are obtained from $\overline{\psi}$ and $\overline{K}$ of each layer, which are calculated at the beginning of each computational time step using the Van Genuchten soil characteristic relationships (Eqs. (37)–(40)) soil hydraulic model. The time derivative or slope of the function $\overline{\theta}_i(t)$ at the beginning of the computational time interval (Euler's slope) is expressed as

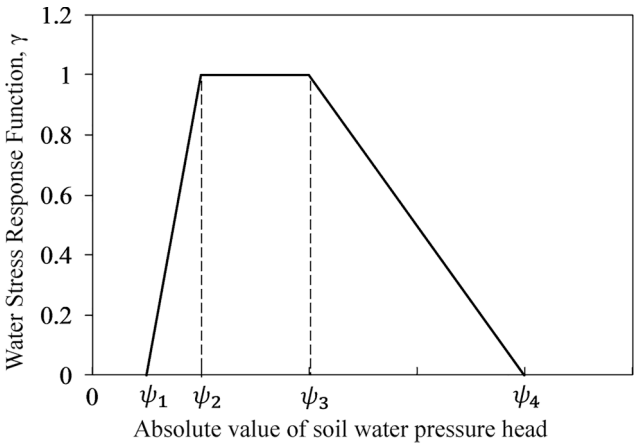

Fig. 2. Schematic of the plant water stress response function (Eq. (41)).

$$\frac{d\overline{\theta}_i}{dt} = f\left(t_j, q_n{}^j\right) \tag{43}$$

where, subscript i denotes layer number; subscript j indicates time t_j; and $f\left(t_j, q_n{}^j\right)$ can be deduced from Eqs. (7) and (9) after arranging terms; it is evaluated at the beginning of the computational time step (t_j). Eq. (43) is used to extrapolate $\overline{\theta}_i$ linearly to the end of the computational time step

$$\overline{\theta}_i^0 = \overline{\theta}_i^j + f\left(t_j, q_n{}^j\right)\Delta t \tag{44}$$

in which the superscript 0 refers to the intermediate prediction of $\overline{\theta}_i$ at time t_{j+1}, which refers to the standard Euler method and Δt is the computational time step [T], $\Delta t = t_{j+1} - t_j$. The fluxes per unit area q_n^0 are obtained from $\overline{\psi}_i^0$ and $\overline{K}_i^0$ which are calculated from $\overline{\theta}_i^0$ and Van Genuchten soil characteristic model. The slope of the function $\overline{\theta}_i(t)$ at the end of the time interval is given by:

$$\frac{d\overline{\theta}_i}{dt} = f\left(t_{j+1}, q_n{}^0\right) \tag{45}$$

where, the superscript $j + 1$ refers to time t_{j+1}. The correction for the prediction (44) is calculated using the average slope for the interval:

$$\overline{\theta}_i^{j+1} = \overline{\theta}_i^j + \frac{f\left(t_j, q_n{}^j\right) + f\left(t_{j+1}, q_n{}^0\right)}{2}\Delta t \tag{46}$$

The slope in (45) is updated based on this correction ($\overline{\theta}_i^{j+1}$) and a revised correction is obtained using (46) once again. These steps are repeated until convergence. A termination criterion, ε, for the convergence of the corrector is provided by:

$$\left|\overline{\theta}_i^{j+1,p} - \overline{\theta}_i^{j+1,p-1}\right| \le \varepsilon \tag{47}$$

where, $\overline{\theta}_i^{j+1,p-1}$ and $\overline{\theta}_i^{j+1,p}$ are the results from the prior iteration and the present correction.

2.7. Model evaluation

We evaluated the two-layer model by comparing scenario simulations of volumetric moisture content and fluxes with corresponding HYDRUS layer-averaged results for three soil textures with various prescribed upper and bottom BCs as well as a moving water table. The selected soil textures were with high, moderate, and low permeability according to their saturated hydraulic conductivity: sandy loam, loam, and clay loam, respectively. The van Genuchten soil hydraulic characteristics model was used for calculating unsaturated hydraulic conductivity and pressure head. The soil characteristics properties of the three soil textures are shown in Table 1. The thickness of the first layer and depth to the water table were set to $h = 10$ cm and $H =$ 40cm. The upper BCs (q_0) involved two combinations of precipitation and potential transpiration (T_p) scenarios (Table 2). Soil evaporation was not considered in model comparison owing to the different ways this model and HYDRUS estimate actual evaporation. We assumed that the vegetation cover was pasture, for which the root water uptake parameters ψ_1, ψ_2, ψ_3, and ψ_4 in the water stress response function were set to the values obtained from Wesseling et al. (1991), which were: 10 cm, 25 cm, 800 cm, and 8000 cm, respectively. We considered three distinct water table

Table 1
Soil properties for van Genuchten model (Carsel and Parrish, 1988).

Soil type	α (cm^{-1})	n	θ_r (cm^3 cm^{-3})	θ_s (cm^3 cm^{-3})	K_s (cm day^{-1})	λ
Sandy Loam	0.075	1.89	0.065	0.41	106.1	0.5
Loam	0.036	1.56	0.078	0.43	24.96	0.5
Clay loam	0.019	1.31	0.095	0.41	6.24	0.5

Table 2
Upper boundary conditions.

Scenario #	Rainfall intensity i (cm/day)	Potential transpiration rate T_p (cm/day)
1	0	0.2
2	0.5	0

(WT) scenarios: 1) free-drainage at depth H (deep WT); 2) WT at depth H below the root zone; and 3) dynamic WT: sudden rise of WT to the surface and exponential decline afterward. The third scenario exemplifies the capability of the model to simulate desaturation of the two soil layers. For the shallow WT scenario, we imposed zero-pressure head BC (Eq. (31)) assuming $\psi_b = 0$. The initial moisture contents for three soil textures were set to 80% of effective saturation rate (S_e). Simulations were performed for a 20-day period with 0.001 days of computational time step (about 1.44 min).

In scenario 3, we hypothesize that the soil domain is instantly saturated by a sudden rise of the WT from initial depth $H_0 = 40$ cm to $H = 0$ at the soil surface at time t = 0 days followed by a gradual desaturation. During desaturation, we assume an exponential decline of the WT to its initial depth H_0:

$$H(t) = H_0\left(1 - e^{-0.03t}\right) \tag{48}$$

This scenario was simulated for 100 days with a computational time step of 0.001 days. Without loss of generality, the upper BC was set to zero rain and zero evapotranspiration.

HYDRUS (Šimůnek et al., 2005) was used as a benchmark to evaluate the two-layer model performance. HYDRUS software package is a computer-based program, which implements the finite element method for spatial discretization, has been widely and successfully applied in simulating water flow in porous media, and it has been tested by extensive studies showing that it provides trustworthy results in terms of estimating soil moisture content and water flux (Caiqiong and Jun, 2016; Kornelsen and Coulibaly, 2014; Liu et al., 2018; Mohammadzadeh-Habili and Heidarpour, 2015; Sellers et al., 1986). Therefore, HYDRUS is often used as the benchmark model to verify proposed numerical schemes (e.g., Baiamonte, 2020; Ogden et al., 2015; Lai and Ogden, 2015; Sadeghi et al., 2019; Zhang et al., 2016). The finite element mesh applied here in HYDRUS was constructed by discretizing the soil profile into 101 elements. Because HYDRUS solves RE at multiple discretized nodes, the averaged water contents for two soil layers were calculated by summing the values of water contents over all nodes and dividing by the number of nodes within each layer (nodes are evenly spaced in each layer). The time step used in HYDRUS was the same as that used in the two-layer model for each simulation scenario. For consistency, the adaptive time-stepping scheme was not implemented in HYDRUS. The tolerance in convergence criterion between the iterations (Eq. (47)) was set to the water content difference of 0.0001 in both the two-layer model and HYDRUS. We used root mean square error (*RMSE*) to measure the model performance. In practice, the precision of the in-situ soil moisture measurement probes is assumed to be good for $RMSE \le 0.02$ (Robinson et al., 2008).

$$RMSE = \sqrt{\frac{1}{N}\sum_{i=1}^{N}\left(\theta^*{}_i - \theta_{HYDRUS,i}\right)^2} \tag{49}$$

where, $\theta^*{}_i$ is the i^{th} simulated soil moisture by the two-layer model; $\theta_{HYDRUS,i}$ is the i^{th} simulated value by HYDRUS; and N is number of simulated days.

3. Results

Overall, the two-layer model simulated layer-averaged moisture contents compared very well with those obtained by integrating the

nodal values calculated by HYDRUS.

3.1. Free-drainage BC

Soil moisture contents and fluxes simulated by the two-layer model compared well to the corresponding layer-averaged HYDRUS results with free-drainage BC (Figs. 3 and 4). The *RMSE* values for layer-averaged θ were between 0 to 0.010 and 0 to 0.011 for the first and the second layers, respectively (Table 3). Coarse textured soil (sandy loam) showed the fastest rate to reached steady than fine-textured soils, as the moisture content plots in Figs. 3 and 4 show. The estimated moisture content of the second layer by the two-layer model compared better with corresponding HYDRUS values under rainfall scenario (i = 0.5 cm/day, T_p = 0 cm/day) (Fig. 3) than the scenario of plant water uptake by transpiration (i = 0 cm/day, T_p = 0.2 cm/day) (Fig. 4).

The top and bottom cumulative flux values of the three soils agreed well with those simulated by HYDRUS. The fluxes were identical to those from HYDRUS (e.g. Fig. 4b). The temporal behavior of water flux at both boundaries was well captured by the two-layer model. Computed cumulative fluxes in the rainfall scenario had a much better match with those from HYDRUS than for the transpiration-only scenario. The two-layer model and HYDRUS initially estimated cumulative transpiration at the potential rate, when the soil water potential was between ψ_2 and ψ_3, as depicted by the linear trend in Fig. 3. When soil moisture of the root zone decreased by the influences of plant extraction and gravity, transpiration rate started to decrease at the time when water potential reached the range between ψ_3 and ψ_4. The two-layer model estimated cumulative transpiration was larger than those estimated by HYDRUS in the transition period toward steady-state values (from about 10 days to 20 days for sandy loam and after about 15 days for loam and clay loam soil in Fig. 3b). The two-layer model estimated cumulative transpiration compared better in loam and clay loam than in sandy loam. For sandy loam, the lower values of the average soil moisture in the second layer after 10 days was contributed by higher estimated transpiration rates in the two-layer model (Fig. 3a). The near flat bottom cumulative flux in the second layer implies free drainage has seized after 10 days and the continued decrease of computed average moisture thereafter can only be explained by the second layer contributing to simulated plant uptake in the first layer (root zone).

3.2. Zero-pressure BC (Water Table)

With zero-pressure head BC (Eq. (31)), the water table can exchange moisture with the second layer and becomes a source of water moisture to the overlying soil during dry periods. The *RMSE* values for layer-averaged θ ranged between 0.001 to 0.006 and 0.001 to 0.008 for the first and the second layers, respectively (Table 3). Similar to the free-drainage scenario, the two-layer mode results for soil water content and cumulative fluxes were in a very good agreement with those obtained from HYDRUS with groundwater at the bottom of the soil domain. In this scenario, the second layer receives water from the saturated zone and contributes flux to the first layer to meet plant water demand. Except for sandy loam in layer 1 where free drainage dominated, comparison of Fig. 4(a) with Fig. 6(a) and Fig. 3(a) with Fig. 5(a) shows the effect of shallow water table on moisture build-up in both layers. All simulations reached steady-state relatively fast (in two days). For clay loam, the two-layer model reached steady state faster than HYDRUS with the transpiration scenario, but was slower with the rainfall scenario. Computed cumulative fluxes by the two-layer model were in perfect match with those from HYDRUS. Both models simulated transpiration rates at the potential rate in all simulations as the root zone matric potentials were between ψ_2 and ψ_3. This is supported by the

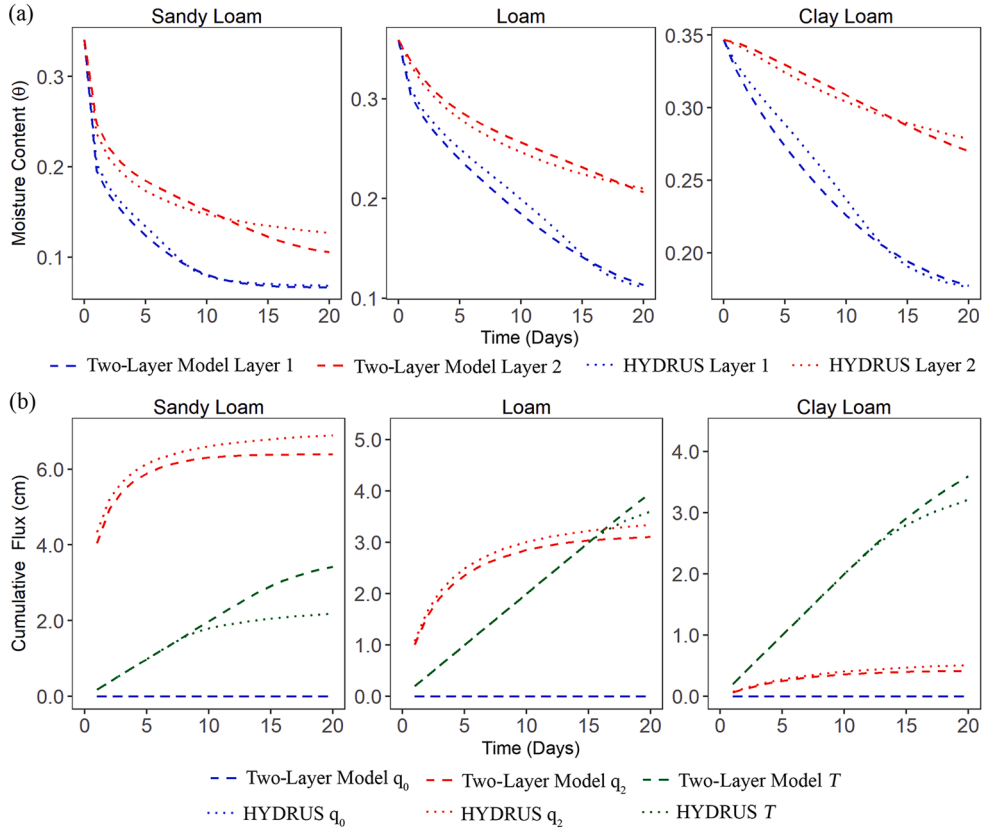

Fig. 3. Moisture contents and cumulative fluxes with free-drainage BC, i = 0 cm/day, T_p = 0.2 cm/day. (a) represents results for soil moisture comparison between two-layer model and HYDRUS; (b) represents results for cumulative top, bottom fluxes and transpiration comparison between two-layer model and HYDRUS; where q_0 and q_2 donate top and bottom flux terms, respectively; T donates actual transpiration).

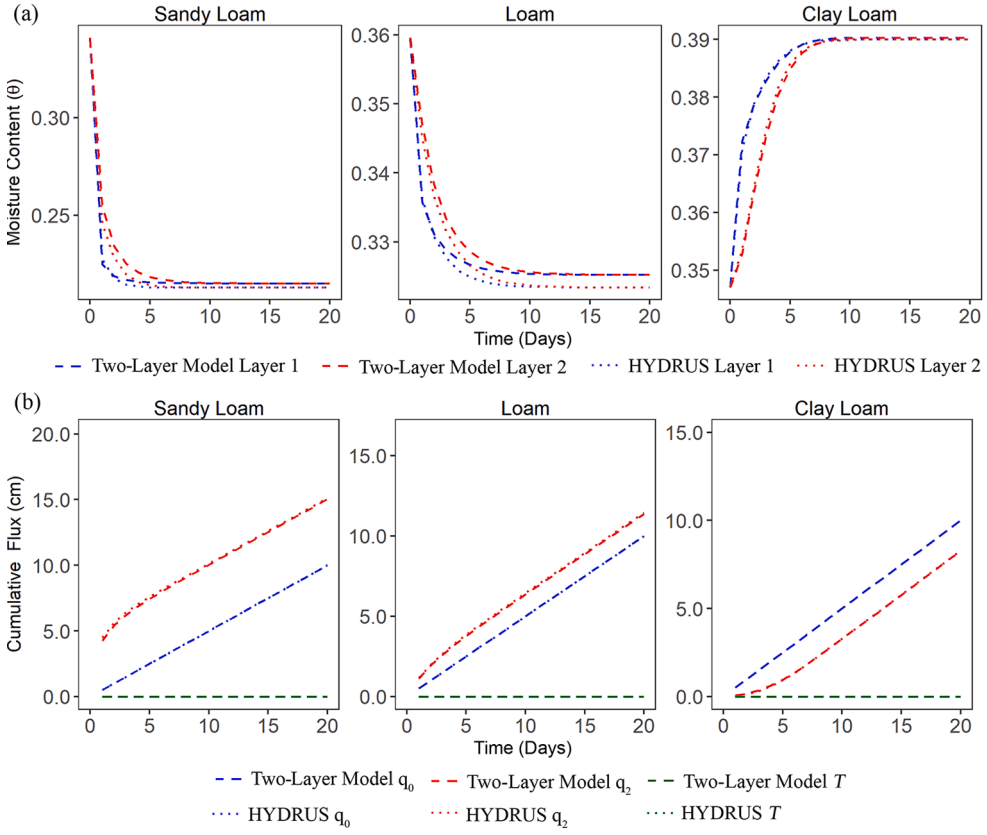

Fig. 4. Moisture contents and cumulative fluxes with free-drainage BC, $i = 0.5$ cm/day, $T_p = 0$ cm/day (note that the top and bottom cumulative fluxes and cumulative transpiration from the two-layer model are overlapped with those from HYDRUS).

Table 3
RMSE of soil moisture content for numerical simulations.

Numerical scenarios	Soil textures	$i = 0$ cm/day, $T_p = 0.2$ cm/day		$i = 0.5$ cm/day, $T_p = 0$ cm/day	
		First layer	Second layer	First layer	Second layer
Free-drainage	Sandy Loam	0.005	0.011	0.002	0.004
	Loam	0.010	0.007	0.002	0.002
	Clay Loam	0.010	0.004	0.000	0.000
Mixed-pressure head	Sandy Loam	0.004	0.008	0.006	0.005
	Loam	0.001	0.001	0.001	0.002
	Clay Loam	0.005	0.004	0.002	0.007
		$i = 0$ cm/day, $T_p = 0$ cm/day			
		First layer		Second layer	
Groundwater decline	Sandy Loam	0.004		0.006	
	Loam	0.001		0.000	
	Clay Loam	0.000		0.000	

computed linear cumulative transpiration in Fig. 5(b).

3.3. Dynamic WT

This hypothetical scenario depicts a sudden rise of WT to the surface at $t = 0$ and subsequent desaturation, assuming an exponential falling rate of the WT (Eq. (48)). Numerical results of soil water contents for sandy loam, loam and clay loam are shown in Fig. 7. Estimated soil moisture for the first and the second layer all showed the same trend with HYDRUS results. The two-layer model showed excellent performance in calculating soil moisture for both layers (Table 3). The differences between the moisture content values estimated by the two models decreased as the soil texture became finer. The evolution of $\overline{\theta}_1$ and $\overline{\theta}_2$ was well captured by the current model. The transition from saturated to unsaturated conditions caused by groundwater decline was well captured with no numerical stability problems. Note the initially steady values of $\overline{\theta}_2$ at saturation until around $t = 9.6$ days when it starts declining. This corresponds to the time when the WT reaches the bottom of layer 1 ($H = 10$ cm) and the ensuing desaturation of layer 2 as the water table continues falling to the original position at depth 40 cm. Before t = 9.6 days, the water table is situated within layer 1, and layer 2 consequently is saturated.

4. Discussion

Soil moisture dynamics is normally governed by solving Richard's elliptic–parabolic partial differential equation or a variant of it. Current numerical models are either too simple to achieve the desired accuracy (e.g., Ducoudré et al., 1993; Neitsch et al., 2011) or too complex, time-consuming, and computationally expensive to implement on large spatial scales and finer temporal resolution (Farthing and Ogden, 2017; Harter et al., 2004; Qi et al., 2018). The vertically-averaged solution to RE describes one-dimensional water movement and soil moisture dynamics averaged over the thicknesses of the root zone and the vadose zone below. The proposed numerical scheme solves for layer-averaged moisture content in each soil zone as opposed to point values (nodal or grid-centered values). This is because the two-layer model is derived based on integrated form of the finite differences approximations and expressed in terms of layer thickness-averaged values. The numerical scheme of the two-layer model involves an adequate parameterization of

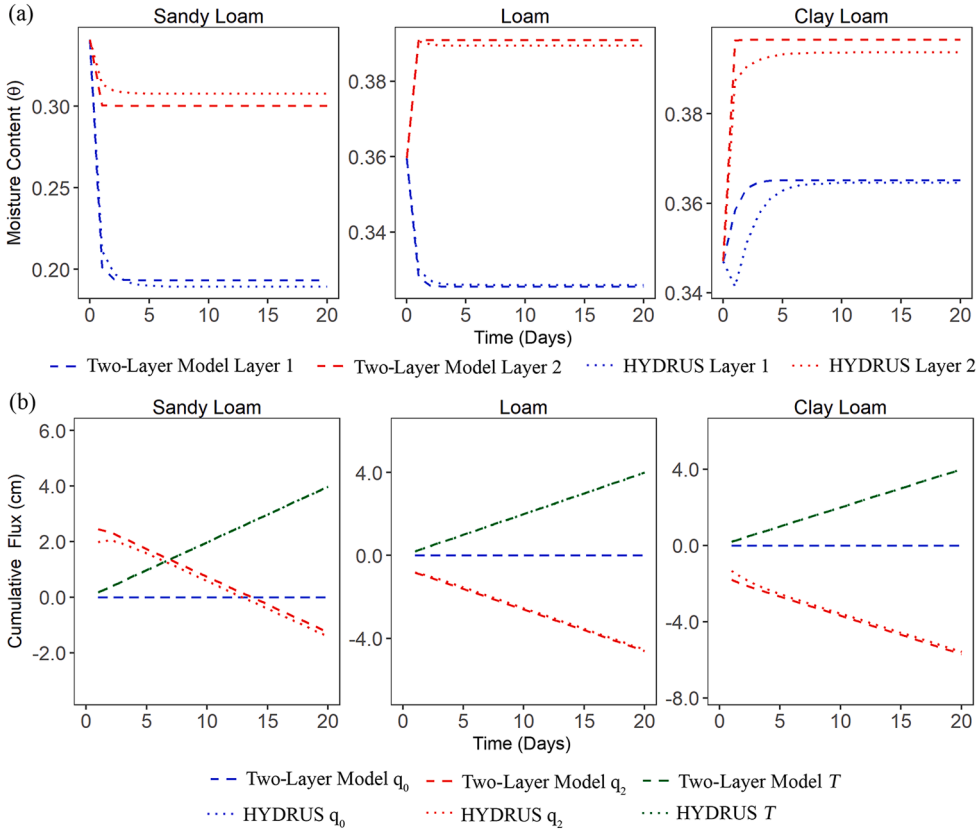

Fig. 5. Moisture contents and cumulative fluxes with zero-pressure head BC, $i = 0$ cm/day, $T_p = 0.2$ cm/day.

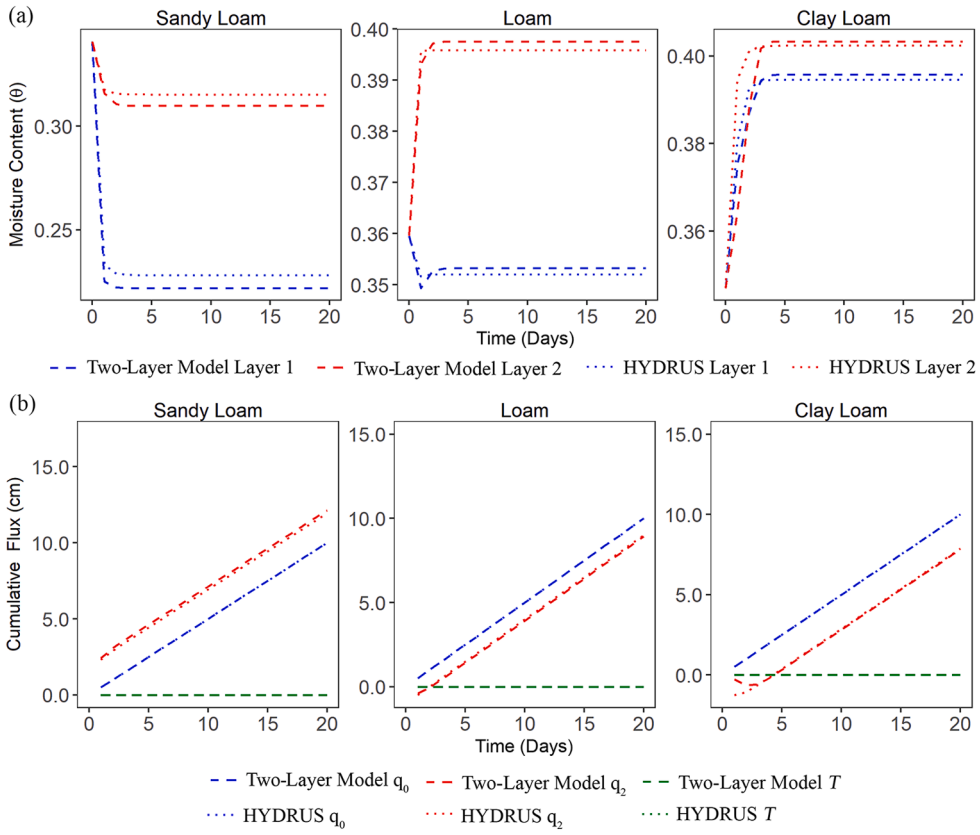

Fig. 6. Moisture contents and fluxes with zero-pressure head BC, $i = 0.5$ cm/day, $T_p = 0$ cm/day.

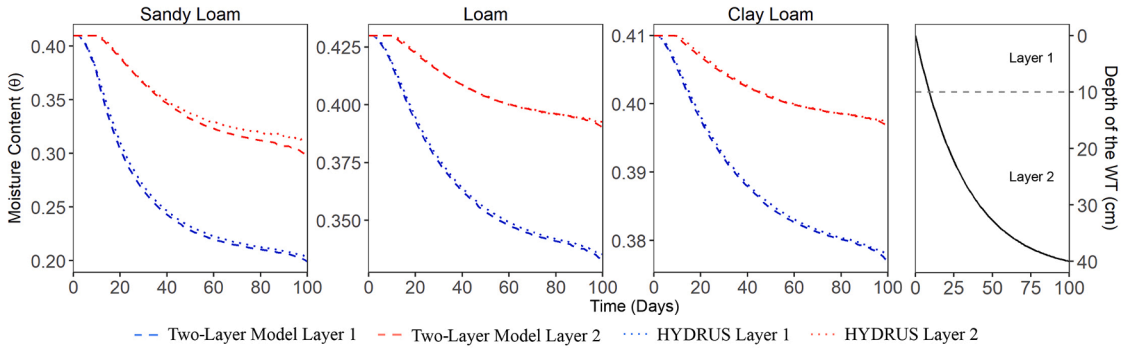

Fig. 7. Moisture contents with declining water table, $i = 0$ cm/day, $T_p = 0$ cm/day.

soil physics and it is relatively simple, stable, and robust. It is accurate and requires less CPU time. The numerical solutions in tested simulations all converged very fast. The predicted top and bottom fluxes as well as plant transpiration compared very well with HYDRUS results for both cases of free-drainage and WT as the bottom BCs. The newly developed two-layer model was able to reproduce salient features of drainage under capillary and gravity forces. The simulation for sandy loam soil showed that coarse soil textures which have relatively high conductivity tend to lose water faster than fine textured soils due to gravity drainage and have moisture content close to wilting point at steady state (Figs. 3(a) and 4(a)). The ability of the two-layer model to simulate supply of moisture from the WT to both layers was evident in fine-textured soils (Figs. 5(a) and 6(a)). Despite the presence of WT, the model simulated quick drainage of the water by gravity in the two layers for sandy loam and loam very well (Figs. 5(a) and 6(a)). When considering water table at the bottom of the soil profile, groundwater can move upward due to suction forces, and the upward flux from the second layer to the first layer is highly determined by the soil characteristics and layer thicknesses. The finer the soil texture, the higher the soil water contents of the first and the second layer at steady state will be. As shown in Figs. 5 and 6, the second layer of clay loam reaches saturated conditions and the moisture content of the first layer stays close to saturation.

The differences between the two-layer model and HYDRUS can be attributed to truncation errors of order $(\Delta z)^2$. The greater the layer thickness the larger the error and the differences with integrated finer-discretization solution computed by HYDRUS (based on 100 cells here). Higher-order corrections might be needed to improve model performance. Moreover, transpiration rate is computed slightly differently in both models. In the two-layer model, plant roots are assumed to be uniformly distributed within the root zone and transpiration is calculated using the layer-averaged capillary pressure head (matric potential), which, in turn, is calculated from layer-averaged soil moisture content using the soil characteristic relationship. In HYDRUS, however, the sink term is described by the plant root water uptake distribution function, which is non-uniformly distributed in the root zone. This could underestimate the computed transpiration rate in some nodes relative to others during the soil drying process. The averaging approach in the two-layer model is producing higher transpiration than that in HYDRUS, although the average soil moisture contents are similar in both models. (see Fig. 3b).

Because only two soil layers are considered in this new model, the two coupled ordinary differential equations involving top, interfacial and bottom fluxes govern water movement in the soil profile. Results showed that Heun's method in the two-layer model is a simple numerical method; it gives stable, robust and relatively accurate results. These simplifications make the computer program taking up less memory and CPU usage than those taken by HYDRUS. In addition, we have tested the 4th order Runge-Kutta method in solving the coupled equations and compared to Heun's method. The results regarding moisture contents for the two soil layers and fluxes (data not shown) matched precisely those obtained using Heun's method. However, the CPU time in Runge-Kutta method was a little longer than the Heun's method. The Runge-Kutta method requires two additional sets of variables compared to Heun's method to allocate the parameters that are used for calculating 3rd and 4th slope. Besides, during the simulation, if the soil moisture change between time steps is small, the numerical solution can converge faster. Four slopes still need to be calculated in one iteration in Runge-Kutta method, while Heun's method only calculates two slopes. Thus, the use of Heun's method with the corrector-predictor algorithm using certain predefined termination criteria in the numerical scheme can ensure the accuracy of the calculation during the iterations and minimize the number of iterations during each time step.

The newly developed two-layer model can be an efficient soil moisture and water fluxes estimation algorithm for coupling surface water and groundwater systems at field and watershed scales or even at larger scales. We showed that the model produces relatively accurate estimations of averaged soil moisture and water fluxes, and is robust enough to account for the effect of fluctuating, shallow water table. Distributed watershed models and land surface models need to perform simulations at hydrologic response unit level or grid level, often for long periods (Fatichi et al., 2016). Therefore, computational cost is something that needs to be accounted for. Input parameters for this new model are relatively less, which makes it easy to set up and function, and thus ideal for large-scale hydrologic modeling. This model is also suitable in applications where groundwater is relatively shallow and where average soil moisture suffices for estimating biogeochemistry in complex ecosystems (e.g., wetlands), and when determining fluxes between surface water and groundwater systems is of interest. Wetland nutrient and carbon cycling models requiring averaged soil moisture content to simulate biochemical processes in variably saturated/unsaturated soils can greatly benefit from this model (Sharifi et al., 2017). In recent years, remote sensing techniques have provided large-scale soil moisture data and continuous surface soil moisture monitoring (Wagner et al., 2013; Babaeian et al., 2018). However, remote sensing observation provides near-surface soil moisture data only (about 0–5 cm). The determination of deeper soil moisture content can be equally important and control water fluxes between the surface water and the groundwater systems (Sadeghi et al., 2019).

5. Summary and conclusions

We have developed a new, stable and robust vertically-averaged form of one-dimensional RE to model vertical unsaturated water movement in a two-layered soil. The two-layer model simulates averaged soil moisture content by connecting hydroclimate conditions to the vadose zone with shallow and deep WTs. The PDE of RE is replaced with two-coupled ODEs and solutions are obtained numerically using the simple Huen's method. A novel feature is the term in the second ODE accounting for a dynamic WT. The numerical method is mass-conservative. The objective of the model is to couple land surface and

aquatic ecosystems to the vadose soil and groundwater to simulate surface water and groundwater interactions at larger than local scales, such as in wetlands and watersheds. At such scales where the areal extent is much greater than the vertical, average fluxes can be well represented by soil moisture averaged over the roots layer and the vadose zone, especially for shallow surficial aquifers. Besides numerical errors caused by truncation of higher-order terms, the model does not simulate horizontal flow nor account for the effect of sloping soil surfaces.

The performance of the two-layer model was investigated in terms of computational accuracy and efficiency by comparison with HYDRUS as a reference model for three simulation scenarios, free drainage at the bottom of the soil profile, WT at the bottom of the soil domain, and falling water table. Three soil textures and different combinations of plant transpiration and rainfall rates were considered. The results showed that the two-layer model was robust and accurate in simulating variably saturated flows. The new model can capture the dynamics of depth-averaged soil moisture under different surface flux BCs in the presence of deep and shallow water table. Overall, simulated cumulative fluxes agreed very well with those from HYDRUS for all scenarios. Although some relatively small discrepancies of moisture estimates between the two models were observed, the *RMSE* values, overall, indicate excellent model performance. Moreover, the two-layer model captured actual evaporation dynamics well in the root zone, mimicking the behavior of the root zone or the biologically active sediment layer in wetlands. Further, numerical simulations conducted for desaturation of an initially saturated soil profile by a falling WT showed that the two-layer model could successfully capture the dynamics of average soil moisture above the water table within the root zone and the lower vadose soil as the WT retreats.

Although the two-layer model proved very promising and accurate under various conditions, there is certainly room for improvement. For instance, while the model has excellent performance when soil layers are relatively shallow, the accuracy drops when soils become deep. Further, natural soils could be very heterogeneous, and thus, soil properties could be highly variable. The current model can only deal with two uniform soil layers. If the soil within the domain consists of more than two soil textures, extra calculations are needed to obtain averaged soil properties for two layers. While recent advances using stochastic theory can furnish formulas for estimating effective properties for use in the two-layer model, this does not negate the errors inherited by truncating higher-order terms and other assumptions made to derive the coupled ODEs.

The CPU times required to run the two-layer model for numerical experiments in this paper were less than that for HYDRUS. The two-layer model has fewer input parameters and uses a simple numerical method, making use of less memory and CPU than finite-element-based RE solutions. For simulations and applications from field-scale to large watershed scale where resolution of water content with depth is not needed, the two-layer model can be a reliable numerical method for simulating soil moisture spatial and temporal variability. This is especially true for watershed simulations involving relatively shallow groundwater and computing biogeochemistry of complex ecosystems. Although simple numerical tests were conducted, the strength and weakness of the two-layer model are not fully comprehended. In a follow-up paper, the model will be investigated in more detail, considering differences in hydraulic properties between the two layers and various surface and bottom BCs. In addition, model predictive uncertainty will be examined by application to field site data where climate and soil moisture data are available at high temporal resolution, along with measured soil properties. This application will provide further evidence on model robustness to simulate moisture content in the field under complex hydroclimate conditions.

CRediT authorship contribution statement

Junhao He: Software, Methodology, Formal analysis, Writing - original draft. **Mohamed M. Hantush:** Conceptualization, Methodology, Writing - review & editing. **Latif Kalin:** Investigation, Methodology, Project administration, Writing - review & editing, Supervision. **Mehdi Rezaeianzadeh:** Methodology, Software. **Sabahattin Isik:** Methodology, Software, Data curation.

Declaration of Competing Interest

The authors declare that they have no known competing financial interests or personal relationships that could have appeared to influence the work reported in this paper.

Acknowledgments

The U.S.EPA through its Office of Research and Development partially funded and collaborated in the research reported in this paper under Contract EP-C-11-010 with Auburn University, School of Forestry and Wildlife Sciences. This document has been reviewed in accordance with U.S. Environmental Protection Agency policy and approved for publication. The views expressed in this article are those of the authors and do not necessarily represent the views or the policies of the U.S. Environmental Protection Agency.

References

Allen, R.G., Pereira, L.S., Smith, M., Raes, D., Wright, J.L., 2005. FAO-56 dual crop coefficient method for estimating evaporation from soil and application extensions. J. Irrig. Drain. Eng. 131 (1), 2–13. https://doi.org/10.1061/(ASCE)0733-9437(2005)131:1(2).

Babaeian, E., Sadeghi, M., Franz, T.E., Jones, S., Tuller, M., 2018. Mapping soil moisture with the OPtical TRApezoid Model (OPTRAM) based on long-term MODIS observations. Remote Sens. Environ. 211, 425–440. https://doi.org/10.1016/j.rse.2018.04.029.

Baiamonte, G., 2020. Analytical solution of the Richards equation under gravity-driven infiltration and constant rainfall intensity. J. Hydrol. Eng. 25 (7), 04020031. https://doi.org/10.1061/(ASCE)HE.1943-5584.0001933.

Belfort, B., Younes, A., Fahs, M., Lehmann, F., 2013. On equivalent hydraulic conductivity for oscillation–free solutions of Richard's equation. J. Hydrol. 505, 202–217. https://doi.org/10.1016/j.jhydrol.2013.09.047.

Bizhanimanzar, M., Leconte, R., Nuth, M., 2019. Modelling of shallow water table dynamics using conceptual and physically based integrated surface-water–groundwater hydrologic models. Hydrol. Earth Syst. Sci. 23 (5), 2245–2260. https://doi.org/10.5194/hess-23-2245-2019.

Caiqiong, Y., Jun, F., 2016. Application of HYDRUS-1D model to provide antecedent soil water contents for analysis of runoff and soil erosion from a slope on the Loess Plateau. Catena 139, 1–8. https://doi.org/10.1016/j.catena.2015.11.017.

Cao, H., Yue, X., 2014. Homogenization of Richards' equation of van Genuchten-Mualem model. J. Math. Anal. Appl. 412 (1), 391–400. https://doi.org/10.1016/j.jmaa.2013.10.063.

Caviedes-Voullième, D., García-Navarro, P., Murillo, J., 2013. Verification, conservation, stability and efficiency of a finite volume method for the 1D Richards equation. J. Hydrol. 480, 69–84. https://doi.org/10.1016/j.jhydrol.2012.12.008.

Celia, M.A., Bouloutas, E.T., Zarba, R.L., 1990. A general mass-conservative numerical solution for the unsaturated flow equation. Water Resour. Res. 26 (7), 1483–1496. https://doi.org/10.1029/WR026i007p01483.

Dai, Y., Zhang, S., Yuan, H., Wei, N., 2019. Modeling variably saturated flow in stratified soils with explicit tracking of wetting front and water table locations. Water Resour. Res. 55 (10), 7939–7963. https://doi.org/10.1029/2019WR025368.

Downer, C.W., Ogden, F.L., 2004a. Appropriate vertical discretization of Richards' equation for two-dimensional watershed-scale modelling. Hydrol. Process. 18 (1), 1–22. https://doi.org/10.1002/hyp.v18:110.1002/hyp.1306.

Downer, C.W., Ogden, F.L., 2004b. GSSHA: model to simulate diverse stream flow producing processes. J. Hydrol. Eng. 9 (3), 161–174. https://doi.org/10.1061/(ASCE)1084-0699(2004)9:3(161).

Ducoudré, N.I., Laval, K., Perrier, A., 1993. SECHIBA, a new set of parameterizations of the hydrologic exchanges at the land-atmosphere interface within the LMD atmospheric general circulation model. J. Clim. 6 (2), 248–273.

Farthing, M.W., Ogden, F.L., 2017. Numerical solution of Richards' Equation: a review of advances and challenges. Soil Sci. Soc. Am. J. 81 (6), 1257–1269. https://doi.org/10.2136/sssaj2017.02.0058.

Farthing, M.W., Kees, C.E., Coffey, T.S., Kelley, C.T., Miller, C.T., 2003. Efficient steady-state solution techniques for variably saturated groundwater flow. Adv. Water Resour. 26 (8), 833–849. https://doi.org/10.1016/S0309-1708(03)00076-9.

Fatichi, S., Vivoni, E.R., Ogden, F.L., Ivanov, V.Y., Mirus, B., Gochis, D., Downer, C.W., Camporese, M., Davison, J.H., Ebel, B., Jones, N., Kim, J., Mascaro, G., Niswonger, R., Restrepo, P., Rigon, R., Shen, C., Sulis, M., Tarboton, D., 2016. An overview of current applications, challenges, and future trends in distributed

process-based models in hydrology. J. Hydrol. 537, 45–60. https://doi.org/10.1016/j.jhydrol.2016.03.026.
Feddes, R.A., 1982. Simulation of Field Water Use and Crop Yield. Pudoc.
Forsyth, P.A., Wu, Y.S., Pruess, K., 1995. Robust numerical methods for saturated-unsaturated flow with dry initial conditions in heterogeneous media. Adv. Water Resour. 18 (1), 25–38. https://doi.org/10.1016/0309-1708(95)00020-J.
Harter, T., Hopmans, J.W., Feddes, R.A., 2004. Role of Vadose Zone Flow Processes in Regional Scale Hydrology: Review, Opportunities and Challenges. Kluwer.
Hayek, M., 2016. An exact explicit solution for one-dimensional, transient, nonlinear Richards' equation for modeling infiltration with special hydraulic functions. J. Hydrol. 535, 662–670. https://doi.org/10.1016/j.jhydrol.2016.02.021.
Herrada, M.A., Gutiérrez-Martin, A., Montanero, J.M., 2014. Modeling infiltration rates in a saturated/unsaturated soil under the free draining condition. J. Hydrol. 515, 10–15. https://doi.org/10.1016/j.jhydrol.2014.04.026.
Huang, R.Q., Wu, L.Z., 2012. Analytical solutions to 1-D horizontal and vertical water infiltration in saturated/unsaturated soils considering time-varying rainfall. Comput. Geotech. 39, 66–72. https://doi.org/10.1016/j.compgeo.2011.08.008.
Jensen, D.T., Hargreaves, G.H., Temesgen, B., Allen, R.G., 1997. Computation of ETo under nonideal conditions. J. Irrig. Drain. Eng. 123 (5), 394–400. https://doi.org/10.1061/(ASCE)0733-9437(1997)123:5(394).
Kornelsen, K.C., Coulibaly, P., 2014. Root-zone soil moisture estimation using data-driven methods. Water Resour. Res. 50 (4), 2946–2962. https://doi.org/10.1002/2013WR014127.
Kumar, P., 2004. Layer averaged Richard's equation with lateral flow. Adv. Water Resour. 27 (5), 521–531. https://doi.org/10.1016/j.advwatres.2004.02.007.
Kumar, M., Duffy, C.J., Salvage, K.M., 2009. A second-order accurate, finite volume–based, integrated hydrologic modeling (FIHM) framework for simulation of surface and subsurface flow. Vadose Zone J. 8 (4), 873–890. https://doi.org/10.2136/vzj2009.0014.
Lai, W., Ogden, F.L., 2015. A mass-conservative finite volume predictor–corrector solution of the 1D Richards' equation. J. Hydrol. 523, 119–127. https://doi.org/10.1016/j.jhydrol.2015.01.053.
Lee, D.H., Abriola, L.M., 1999. Use of the Richards equation in land surface parameterizations. J. Geophys. Res.: Atmos. 104 (D22), 27519–27526. https://doi.org/10.1029/1999JD900951.
List, F., Radu, F.A., 2016. A study on iterative methods for solving Richards' equation. Comput. Geosci. 20 (2), 341–353. https://doi.org/10.1007/s10596-016-9566-3.
Liu, X., Gao, W., Sun, S., Hu, A., He, Y., He, S., 2018. Responses of soil water dynamic processes and groundwater recharge to irrigation intensity and antecedent moisture in the vadose zone. Hydrol. Process. https://doi.org/10.1002/hyp.13368.
Liu, W., Zhang, Z.H.E., Wan, S., 2009. Predominant role of water in regulating soil and microbial respiration and their responses to climate change in a semiarid grassland. Glob. Change Biol. 15, 184–195. https://doi.org/10.1111/j.1365-2486.2008.01728.x.
Maxwell, R.M., Condon, L.E., 2016. Connections between groundwater flow and transpiration partitioning. Science 353 (6297), 377–380. https://doi.org/10.1126/science:aaf7891.
Mohammadzadeh-Habili, J., Heidarpour, M., 2015. Application of the Green-Ampt model for infiltration into layered soils. J. Hydrol. 527, 824–832. https://doi.org/10.1016/j.jhydrol.2015.05.052.
Neitsch, S.L., Arnold, J.G., Kiniry, J.R., Williams, J.R., 2011. Soil and Water Assessment Tool Theoretical Documentation Version 2009. Texas Water Resources Institute.
Ogden, F.L., Lai, W., Steinke, R.C., Zhu, J., Talbot, C.A., Wilson, J.L., 2015. A new general 1-D vadose zone flow solution method. Water Resour. Res. 51 (6), 4282–4300. https://doi.org/10.1002/2015WR017126.
Ogden, F.L., Allen, M.B., Lai, W., Zhu, J., Seo, M., Douglas, C.C., Talbot, C.A., 2017. The soil moisture velocity equation. J. Adv. Model. Earth Syst. 9 (2), 1473–1487. https://doi.org/10.1002/jame.v9.210.1002/2017MS000931.
Oleson, K.W., Lawrence, D.M., Bonan, G.B., Flanner, M.G., Kluzek, E., Lawrence, P.J., Levis, S., Swenson, S.C., Thornton, P.E., Dai, A., Decker, M., Dickinson, R., Feddema, J., Heald, C.L., Hoffman, F., Lamarque, J.-F., Mahowald, N., Niu, G.-Y., Qian, T., Randerson, J., Running, S., Sakaguchi, K., Slater, A., Stockli, R., Wang, A., Yang, Z.-L., Zeng, Xi, Zeng, Xu, 2010. Technical Description of Version 4.0 of the Community Land Model (CLM). NCAR Technical Note NCAR/TN-478+STR, National Center for Atmospheric Research, Boulder, CO, 257 pp. DOI:10.5065/D6FB50WZ.
Orchard, V.A., Cook, F.J., 1983. Relationship between soil respiration and soil moisture. Soil Biol. Biochem. 15 (4), 447–453. https://doi.org/10.1016/0038-0717(83)90010-X.
Priestley, C.H.B., Taylor, R.J., 1972. On the assessment of surface heat flux and evaporation using large-scale parameters. Mon. Weather Rev. 100, 81–92. https://doi.org/10.1175/1520-0493(1972)100<0081:OTAOSH>2.3.CO;2.
Qi, J., Zhang, X., McCarty, G.W., Sadeghi, A.M., Cosh, M.H., Zeng, X., Gao, F., Daughtry, C.S.T., Huang, C., Lang, M.W., Arnold, J.G., 2018. Assessing the performance of a physically-based soil moisture module integrated within the Soil and Water Assessment Tool. Environ. Modell. Software 109, 329–341. https://doi.org/10.1016/j.envsoft.2018.08.024.
Rahman, M., Rosolem, R., Kollet, S.J., Wagener, T., 2019. Towards a computationally efficient free-surface groundwater flow boundary condition for large-scale hydrological modelling. Adv. Water Resour. 123, 225–233. https://doi.org/10.1016/j.advwatres.2018.11.015.
Rathfelder, K., Abriola, L.M., 1994. Mass conservative numerical solutions of the head-based Richards equation. Water Resour. Res. 30 (9), 2579–2586. https://doi.org/10.1029/94WR01302.
Richards, L.A., 1931. Capillary conduction of liquids through porous mediums. Physics 1 (5), 318–333. https://doi.org/10.1063/1.1745010.
Robinson, D.A., Campbell, C.S., Hopmans, J.W., Hornbuckle, B.K., Jones, S.B., Knight, R., Ogden, F., Selker, J., Wendroth, O., 2008. Soil moisture measurement for ecological and hydrological watershed-scale observatories: a review. Vadose Zone J. 7 (1), 358–389. https://doi.org/10.2136/vzj2007.0143.
Ross, B., 1990. The diversion capacity of capillary barriers. Water Resour. Res. 26 (10), 2625–2629. https://doi.org/10.1029/WR026i010p02625.
Sadeghi, M., Tuller, M., Warrick, A.W., Babaeian, E., Parajuli, K., Gohardoust, M.R., Jones, S.B., 2019. An analytical model for estimation of land surface net water flux from near-surface soil moisture observations. J. Hydrol. 570, 26–37. https://doi.org/10.1016/j.jhydrol.2018.12.038.
Sanchez-Mejia, Z.M., Papuga, S.A., 2017. Empirical modeling of planetary boundary layer dynamics under multiple precipitation scenarios using a two-layer soil moisture approach: an example from a semiarid shrubland. Water Resour. Res. 53 (11), 8807–8824. https://doi.org/10.1002/2016WR020275.
Sellers, P.J., Mintz, Y., Sud, Y.C., Dalcher, A., 1986. A Simple Biosphere Model (SIB) for use within general circulation models. J. Atmos. Sci. 43, 505–531. https://doi.org/10.1175/1520-0469(1986)043<0505:ASBMFU>2.0.CO;2.
Sharifi, A., Hantush, M.M., Kalin, L., 2017. Modeling nitrogen and carbon dynamics in wetland soils and water using mechanistic wetland model. J. Hydrol. Eng. 22, D4016002. https://doi.org/10.1061/(ASCE)HE.1943-5584.0001441.
Šimůnek, J., van Genuchten, M.T., Sejna, M., 2005. The HYDRUS-1D Software Package for Simulating the Movement of Water, Heat, and Multiple Solutes in Variably Saturated Media, Version 3.0, HYDRUS Software Series 1. Department of Environmental Science, University of California Riverside, Riverside, California, USA, p. 270.
Su, L., Wang, Q., Qin, X., Shan, Y., Zhou, B., Wang, J., 2018. Analytical solution of the one-dimensional nonlinear Richards equation based on special hydraulic functions and the variational principle. Eur. J. Soil Sci. 69 (6), 980–996. https://doi.org/10.1111/ejss.12720.
Sulis, M., Paniconi, C., Rivard, C., Harvey, R., Chaumont, D., 2011. Assessment of climate change impacts at the catchment scale with a detailed hydrological model of surface-subsurface interactions and comparison with a land surface model. Water Resour. Res. 47 (1) https://doi.org/10.1029/2010WR009167.
Svyatskiy, D., Lipnikov, K., 2017. Second-order accurate finite volume schemes with the discrete maximum principle for solving Richards' equation on unstructured meshes. Adv. Water Resour. 104, 114–126. https://doi.org/10.1016/j.advwatres.2017.03.015.
van Dam, J.C., Feddes, R.A., 2000. Numerical simulation of infiltration, evaporation and shallow groundwater levels with the Richards equation. J. Hydrol. 233 (1-4), 72–85. https://doi.org/10.1016/S0022-1694(00)00227-4.
van Genuchten, M.T., 1980. A closed-form equation for predicting the hydraulic conductivity of unsaturated soils. Soil Sci. Soc. Am. J. 44 (5), 892–898. https://doi.org/10.2136/sssaj1980.03615995004400050002x.
Varado, N., Braud, I., Ross, P.J., Haverkamp, R., 2006. Assessment of an efficient numerical solution of the 1D Richards' equation on bare soil. J. Hydrol. 323 (1-4), 244–257. https://doi.org/10.1016/j.jhydrol.2005.07.052.
Wagner, W., Hahn, S., Kidd, R., Melzer, T., Bartalis, Z., Hasenauer, S., Figa-Saldaña, J., de Rosnay, P., Jann, A., Schneider, S., Komma, J., Kubu, G., Brugger, K., Aubrecht, C., Züger, J., Gangkofner, U., Kienberger, S., Brocca, L., Wang, Y., Blöschl, G., Eitzinger, J., Steinnocher, K., 2013. The ASCAT soil moisture product: a review of its specifications, validation results, and emerging applications. Meteorol. Z. 22 (1), 5–33. https://doi.org/10.1127/0941-2948/2013/0399.
Wesseling, J.G., Elbers, J.A., Kabat, P., Van den Broek, B.J., 1991. SWATRE: Instructions for input. Internal Note, Winand Staring Centre, Wageningen, the Netherlands.
Zeng, X., Decker, M., 2009. Improving the numerical solution of soil moisture-based Richards equation for land models with a deep or shallow water table. J. Hydrometeorol. 10, 308–319. https://doi.org/10.1175/2008JHM1011.1.
Zha, Y., Yang, J., Shi, L., Song, X., 2013. Simulating One-Dimensional Unsaturated Flow in Heterogeneous Soils with Water Content-Based Richards Equation. Vadose Zone Journal 12. DOI:10.2136/vzj2012.0109.
Zhang, Z., Wang, W., Yeh, T.J., Chen, L., Wang, Z., Duan, L., An, K., Gong, C., 2016. Finite analytic method based on mixed-form Richards' equation for simulating water flow in vadose zone. J. Hydrol. 537, 146–156. https://doi.org/10.1016/j.jhydrol.2016.03.035.
Zhu, Y., Lü, H., Horton, R., Yu, Z., Ouyang, F., 2016. A modified soil moisture model for two-layer soil. Groundwater 54, 569–578. https://doi.org/10.1111/gwat.12387.